ELSEVIER

Journal of Crystal Growth 194 (1998) 16–24

JOURNAL OF CRYSTAL GROWTH

Mechanism of atomic layer epitaxy of AlAs

S. Hirose*, M. Yamaura, A. Yoshida, H. Ibuka, K. Hara, H. Munekata

Imaging Science and Engineering Laboratory, Tokyo Institute of Technology, 4259 Nagatsuda, Midori-ku, Yokohama 226, Japan

Received 11 March 1998; accepted 8 June 1998

Abstract

A systematic study on atomic layer epitaxy (ALE) of AlAs thin films has been carried out by using ethyldimethylamine alane as an Al source. Self-limiting growth modes accompanied by one, two and three monolayers per ALE cycle have been clearly presented. Each growth mode shows unique dependence of growth temperature on carbon contents. We discuss that one monolayer self-limiting growth proceeds with the conventional adsorbate inhibition model, whereas the self-limiting growth with two and three monolayers can only be explained by the formation of metallic Al layers. We also point out that atomic configuration of the layer may depend on the substrate temperature. Kinetic consideration is also given to examine these models.

PACS: 81.05.Ea; 81.15.Tv; 82.20.Pm

Keywords: Atomic layer epitaxy; Self-limiting growth; AlAs; Ethyldimethylamine alane

1. Introduction

Atomic layer epitaxy (ALE) of III–V compounds has been studied for more than a decade in various materials [1–7]. For GaAs, GaP and InAs, ALE is accompanied by the self-limiting growth with the growth rate of one monolayer (ML) per cycle. The mechanism of the growth is explained in terms of either adsorbate inhibition model or selective adsorption model. Adsorbate inhibition model is that metalorganic adsorbates inhibit any further decomposition of $M(CH)_x$ (M = Ga, In; $x = 1, 2, 3$) precursors on the surface when the surface is fully covered by the adsorbates. The selective adsorption model is that the adsorption of $Ga(CH)_x$ precursors stops by itself when the surface is fully covered with metallic Ga.

As to the Al-based III–Vs, the self-limiting growths of AlAs with 1-, 2-, and 3-ML/cycle have been observed with different source materials and supply conditions. This behavior has been known to be unique for AlAs. For example, Ozeki et al. have observed 1-, 2- and 3-MLs self-limiting growth (SLG) modes using trimethylaluminum [8]. Yokoyama et al. [9] and Fujii et al. [10] have reported 1- and 2-ML SLG modes using cracked triethylaluminum and trimethylamine alane, respectively. Our earlier experiments have demonstrated the ALE with 1- and 2-ML SLG modes

* Corresponding author. Fax: +81 45 924 5175; e-mail: hirose@isl.titech.ac.jp.

0022-0248/98/$ – see front matter
PII: S0022-0248(98)00602-2

using dimethylaluminum hydride [11,12], and 1-, 2-, 3-ML SLG modes with ethyldimethylamine alane (EDMAAl) [13,14]. These results suggest that the multi-ML growth modes are not the problem of choice of source materials, but rather have their origin in the nature of the Al–AlAs surface. The contribution of steric-hindrance effect is probably not also significant.

The aim of this paper is to describe systematically the experimental results on ALE of AlAs, and to build appropriate growth model that can explain multi-ML SLG modes. On the bases of the observed dependence of growth parameter on carbon contents, we propose two types of different growth modes depending on growth condition; one is alkyl-group-terminated 1-ML SLG mode which corresponds to the conventional adsorbate inhibition model, and another is the metallic surface model for 2- and 3-ML SLG modes which may be close to the selective adsorption model.

2. Experimental procedure

A horizontal, low-pressure metal organic vapor phase epitaxy system has been used for experiments. The reactor pressure during ALE growth was maintained at 10 Torr. Details of this reactor have been described in the separate paper [13]. The total flow rate, being predominated by the rate of H_2 carrier gas, was 5 l/min. The reactor was designed to achieve a high flow velocity (90 m/s) to eliminate unwanted gas phase pre-reactions. This makes it possible to expand the ALE temperature window towards high temperatures because the thermal decomposition in gas phase is sufficiently suppressed.

Source materials were arsine (AsH_3), trimethylgallium ($(CH_3)_3Ga$; TMGa), and ethyldimethylamine alane ($C_2H_5(CH_3)_2N{:}AlH_3$; EDMAAl), for arsenic, gallium, and aluminum, respectively. A 100-nm-thick buffer GaAs layer was first grown on a Cr-doped semi-insulating GaAs(0 0 1) substrate by the conventional MOVPE methods at 600°C. A 20–450-nm-thick AlAs layer was then grown by means of ALE method. After the growth of the ALE-AlAs layer, a 100-nm-thick GaAs cap layer was grown on top of AlAs layers by the MOVPE method to protect the AlAs layer from the oxidation.

For the ALE of AlAs, one ALE cycle consisted of four steps: (i) hydrogen (H_2) supply for 3 s, (ii) EDMAAl supply for 1–20 s, (iii) the second H_2 supply for 3 s, and (iv) AsH_3 supply for 10 s. The EDMAAl supply rate was changed between 3.7×10^{-3} and 3.7×10^{-2} μmol/s, while AsH_3 supply rate was fixed at 3.0×10^{1} μmol/s. Growth temperature was varied between 150 and 650°C.

AlAs epilayers were characterized by double-crystal X-ray diffraction (XRD), secondary ion mass spectrometry (SIMS), and scanning electron microscopy (SEM) to evaluate lattice spacing, carbon incorporation, and growth rate, respectively.

3. Experimental data and growth model

We start with discussing the growth rate of AlAs per source supply cycle. Fig. 1 shows the growth rate as a function of substrate temperature (T_s). For $T_s > 300$°C, 1-, 2- and 3-ML self-limiting growths (SLGs) take place for different EDMAAl supply rates (R) of 7.4×10^{-3}, 1.3×10^{-2} and 3.7×10^{-2} μmol/s, respectively. The ALE windows for the SLG are extremely wide compared to the ALE-window of other III–V and II–IV compound semiconductors. This suggests that Al-based metal-organic adsorbates are stable for wide range of T_s.

Growth rates as a function of EDMAAl supply rate (R) and EDMAAl pulse duration (D) are

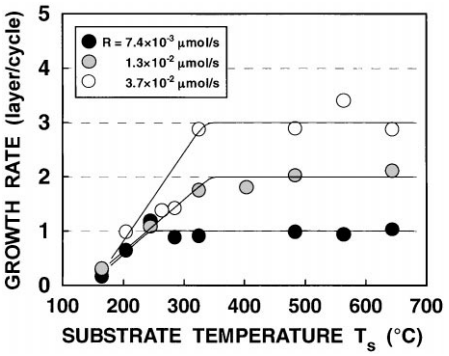

Fig. 1. Growth rates per ALE cycle as a function of T_s for three different EDMAAl supply rates.

shown in Figs. 2 and 3, respectively. Here, T_s was fixed at 480°C. The existence of 1-, 2- and 3-ML SLG is clearly observed again. We can see that the change in the growth rate occurs gradually from 2-ML to 3-ML saturation region, whereas the changes from zero to 1-ML, and from 1-ML to 2-ML are somewhat abrupt. Surface morphology also depends on the growth mode; the surfaces of AlAs layers grown at 1- and 2-ML SLG modes are smooth, whereas the layers grown with the 3-ML SLG mode exhibit rather rough surfaces. This suggests that 1- and 2-ML growths proceed with layer-by-layer growth mode, while 3-ML growth might involve three-dimensional island growth mode.

The (0 0 2) X-ray diffraction data show clearly the difference among the growth modes in terms of carbon incorporation. Fig. 4a–Fig. 4c show the data for a series of AlAs layers grown under 1-, 2-, and 3-ML SLG modes at different growth temperatures (T_s). As to the 1-ML SLG (Fig. 4a), the (0 0 2) diffraction peaks of the epilayers grown at $T_s = 290$ and 330°C appears at the higher-angle side of that of a GaAs substrate. This indicates the reduced lattice constant due to the incorporation of the high amount of carbon, e.g., $[C] = 2.4 \times 10^{19}\,cm^{-3}$ from SIMS analysis using the control sample.[1] When T_s is increased, the peak shifts toward lower-angle side, reflecting the reduced carbon concentration. For the AlAs layer grown at $T_s = 560$°C, the AlAs peak ($2\theta = 31.563°$) appears at the position very close to a thin, undoped AlAs layer grown coherently on a GaAs substrate [13,14]. SIMS analysis gives $[C] = 1.2 \times 10^{18}\,cm^{-3}$ for this sample.

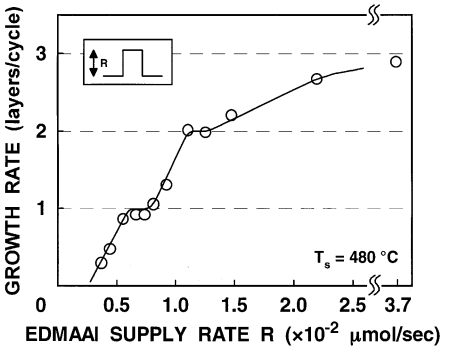

Fig. 2. Growth rates per ALE cycle as a function of EDMAAl supply rate (R).

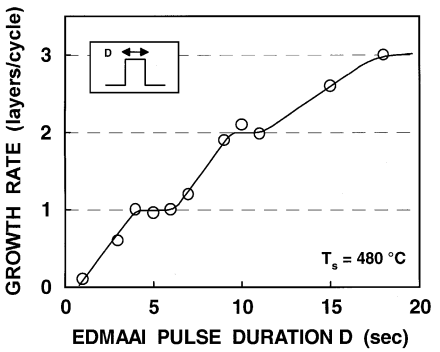

Fig. 3. Growth rates per ALE cycle as a function of EDMAAl pulse duration (D).

In contrast, for the 3-ML SLG, the behavior of the AlAs diffraction peak is totally opposite to that of the 1-ML SLG, as shown in Fig. 4c. The diffraction peak ($2\theta = 31.577°$) from the epilayer grown at $T_s = 290$°C locates at the lower-angle side of the GaAs (0 0 2) peak, and shifts toward higher angles with increasing T_s. This indicates an increase in carbon concentration with increasing the T_s; e.g., carbon concentrations are 1.2×10^{18} and $2.4 \times 10^{19}\,cm^{-3}$ for epilayers grown at $T_s = 290$ and 560°C, respectively. The full-width at half-maximum of the peak also increases with T_s, showing the deterioration of crystalline quality.

As to the 2-ML SLG, the behavior of diffraction peak is rather complex. As shown in Fig. 4b, the diffraction peak for $T_s = 250$°C locates at the position close to the value for a pure, coherently grown AlAs. The peak gradually shifts toward higher angles for $T_s = 330$, 480°C, whereas it comes back toward lower angles at $T_s = 640$°C. Carbon concentration of the epilayers grown at $T_s = 640$°C is estimated to be about $2.0 \times 10^{18}\,cm^{-3}$. These results suggest that the mechanism for each SLG mode involves different surface process.

We now discuss the possible growth mechanism of multi-ML SLG modes (Figs. 5 and 6). Based on the fact that carbon concentration decreases with

[1] AlAs:C control sample was prepared by ion implantation in Prof. Tsutsi's laboratory, Tokyo Institute of Technology.

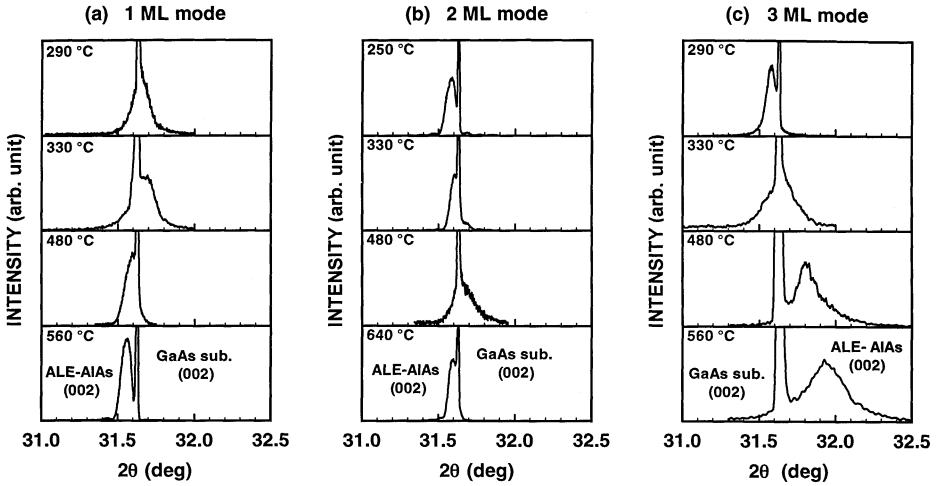

Fig. 4. X-ray (0 0 2) diffraction data of ALE-AlAs layers grown at different T_s for (a) 1-ML, (b) 2-ML and (c) 3-ML SLG modes.

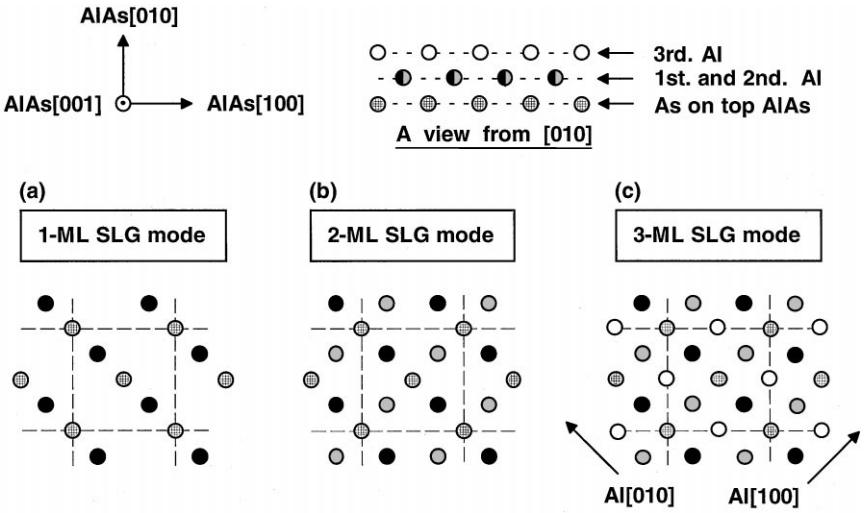

Fig. 5. Schematic illustration of proposed AlAs SLG model at relatively low T_s for (a) 1-ML, (b) 2-ML and (c) 3-ML.

increasing T_s, the 1-ML SLG mode can probably be explained by the conventional, GaAs-type adsorbate inhibition model [2]. Concretely stated, 1-ML of metalorganic aluminum adsorbates cover the surface until they impede excess molecules to be further adsorbed on the surface. Al atoms on the substrate surface presumably occupy the group-III sub-lattice sites of the zinc-blende structure, forming rather strong Al–As tetrahedral covalent bonds (Fig. 5a). When T_s is relatively low, alkyl groups may not be fully released by AsH_3 supply, resulting in the relatively high carbon concentration. Increasing the T_s promotes the surface chemical reaction including the desorption process of alkyl groups from the surface, so that carbon concentration in AlAs layers is decreased.

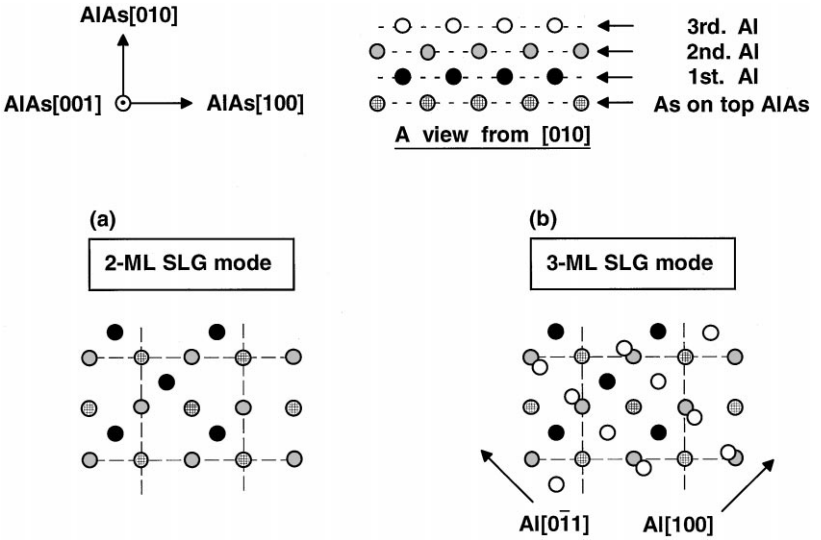

Fig. 6. Schematic illustration of proposed AlAs SLG model at relatively high T_s for (a) 2-ML and (b) 3-ML.

When EDMAAl supply rate (R) is increased, Al atoms are forced to stick on the Al-stabilized AlAs surface, and start forming the second ML. Taking into account the relatively low carbon concentration for the sample grown at $T_s = 250°C$ under 2-ML SLG mode, the mechanism for the 2-ML SLG mode is probably totally different from that for the 1-ML SLG mode. What would happen is the metallization of the surface, involving gradual transformation from the zinc-blende type Al surface to the face-center-cubic (fcc) type Al surface, namely, extra Al atoms occupy the middle points of Al atoms which originally belong to the zinc-blende type 1-ML. This process will result in the formation of 1-ML of fcc type Al(0 0 1) plane, as shown in Fig. 5b. This type of Al surface has been observed in the study on molecular beam epitaxy (MBE) of Al/GaAs(0 0 1) at relatively low T_s [15]. Note that the number of Al atoms per unit cell is twice as high as that of the zinc-blende AlAs, so that 2-ML of AlAs is formed when AsH_3 is supplied to the 1-ML of fcc Al(0 0 1). In terms of the formation of metallic surface, the concept of this picture is close to the selective adsorption model.

Reflecting the metallic nature of the surface, the mechanism of carbon incorporation is also different from that of 1-ML SLG mode. Once the strong Al–C bonds are formed in metallic Al layers due to the decomposition of residual alkyl groups, carbon might be hardly removed even during the supply of AsH_3. Since the decomposition rate of residual alkyl groups increases with increasing the T_s, carbon contents increase accordingly with increasing the T_s. However, at high T_s ($T_s \sim 640°C$), reduction of carbon concentration is observed (Fig. 4b). This suggests the change in the ALE process from the selective-adsorption type to the adsorbate inhibition type. One intriguing picture is to imagine that 2-ML of Al atoms might occupy group III-sub-lattice sites (Fig. 6a) whose top is partially terminated by alkyl group. There is one experimental evidence so far to support this idea [16,17].

For 3-ML SLG mode, we infer, on the basis of the observed T_s dependence on carbon incorporation, that the growth proceeds with either metallic (fcc) Al(0 0 1) or Al(1 1 0) surfaces, depending on T_s. At low T_s region, the Al(0 0 1) may be a preferable atomic configuration (Fig. 5c) because it can maintain the epitaxial relationship on top of the existing 1-ML of Al(0 0 1). At high T_s region, Al(1 1 0) surface (Fig. 6b) may be established as was the case for MBE of Al on the AlAs(0 0 1) surface [15–18]. In fact, we have observed the Al(1 1 0) peak in X-ray diffraction for a 720 nm-Al/AlAs/GaAs(0 0 1)

sample grown by MOVPE at $T_s = 640°C$. In any two cases, the diffusion constant of As in metallic Al is larger than that in covalent AlAs [19], making it possible to form AlAs of around 3-ML-thickness by intermixing reaction with AsH_3. When well-packed metallic Al plane are formed, Al atoms may deposit continuously with further supply of Al source, so that SLG of AlAs does not occur any more. This is why there has been no report for the SLG of more than four monolayers.

4. Kinetic consideration

On the basis of the above-mentioned model, we have examined the dependence of Al pulse duration (D) on growth rate by solving rate equations. As shown in Fig. 7, the growth rate for each ML consists of three different steps: adsorption, nucleation and desorption steps. The adsorption is the step in which thermally decomposed EDMAA1 precursors are adsorbed on the surface. The nucleation is the step in which the adsorbed precursors are incorporated in the crystal in the form of AlAs. The desorption is the step in which excess precursors move away from the surface. These steps are expressed as follows:

$$\frac{dm_1}{dt} = \frac{1 - a_1 - m_1}{\tau_{ads\ 1}} - \frac{m_1}{\tau_{nuc\ 1}} - \frac{m_1}{\tau_{des\ 1}}, \quad (1)$$

$$\frac{dm_2}{dt} = \frac{a_1 - a_2 - m_2}{\tau_{ads\ 2}} - \frac{m_2}{\tau_{nuc\ 2}} - \frac{m_2}{\tau_{des\ 2}}, \quad (2)$$

$$\frac{dm_3}{dt} = \frac{a_2 - a_3 - m_3}{\tau_{ads\ 3}} - \frac{m_3}{\tau_{nuc\ 3}} - \frac{m_3}{\tau_{des\ 3}}, \quad (3)$$

and

$$\frac{da_n}{dt} = \frac{m_n}{\tau_{nuc\ n}} \quad (n = 1, 2 \text{ and } 3). \quad (4)$$

Here, m_n is the surface density of adsorbed Al-contained alkyl species, and a_n being Al atoms which are incorporated in the AlAs crystal. $\tau_{ads\ n}$ (s), $\tau_{nuc\ n}$ (s) and $\tau_{des\ n}$ (s) are the time constants of adsorption, nucleation and desorption, respectively. The first, second and third terms on the right-hand side of Eqs. (1)–(3) indicate the adsorption rates, the nucleation rates, and the desorption rates. The growth rate for each layer is represented by Eq. (4). The total growth rate (GR) is given by solving Eqs. (1)–(4):

$$GR = \sum_n a_n \quad (n = 1, 2, \text{ and } 3). \quad (5)$$

In the conventional MOVPE of AlAs, adsorbed Al-species are changed quickly to Al atoms on the surface due to the presence of excess AsH_3. Therefore, the growth rate increases linearly with

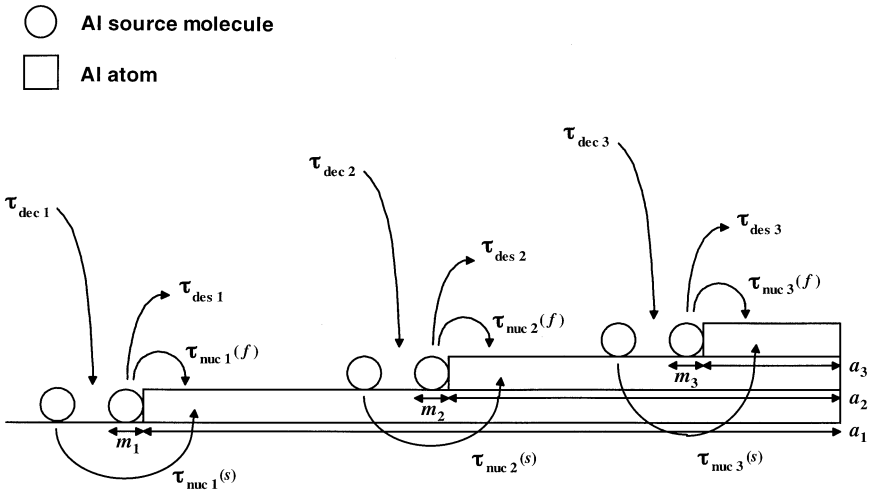

Fig. 7. Schematic illustration of surface reaction process for each ML layer.

increasing D. When the value of $\tau_{\mathrm{ads}\,n}$, $\tau_{\mathrm{nuc}\,n}$ and $\tau_{\mathrm{des}\,n}$ ($n = 1$, 2 and 3) are chosen to be 1.0×10^{-3}, 1.0×10^{-6} and 1.0×10^{-2} s, respectively, we obtain the line (A) in Fig. 8a. This corresponds to the MOVPE growth rate of 0.3 μm/h realized in our reactor with the EDMAAl supply rate (R) of 3.7×10^{-3} μmol/s. Time constants used in the calculations are listed in Table 1.

To calculate the actual ALE growth rate, we take into account the existence of atomic step, because the rate of nucleation is usually faster for Al atoms which are in the vicinity of the steps than for those which are remote from the steps. On the basis of this inference, we divide the total nucleation rate into two components; the slower ($\tau_{\mathrm{nuc}\,n}(s)$) and faster ($\tau_{\mathrm{nuc}\,n}(f)$) ones. Therefore, $\tau_{\mathrm{nuc}\,n}$ are expressed as follows:

$$\frac{1}{\tau_{\mathrm{nuc}\,1}} = \frac{1-a_1}{\tau_{\mathrm{nuc}\,1}(s)} + \frac{a_1}{\tau_{\mathrm{nuc}\,1}(f)}, \tag{6}$$

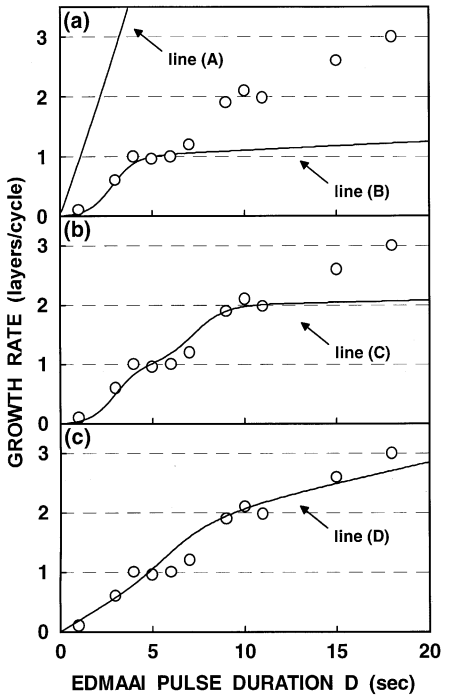

Fig. 8. Growth rate per ALE cycle as a function of EDMAAl pulse duration (D). Lines (A), (B), (C) and (D) are of calculated data for MOVPE, 1-ML ALE, 1- and 2-ML ALE, and 3-ML ALE, respectively.

Table 1
Time constants τ (s) which are used to reproduce experimental data

	$\tau_{\mathrm{ads}\,1}$	$\tau_{\mathrm{ads}\,2}$	$\tau_{\mathrm{ads}\,3}$	$\tau_{\mathrm{des}\,1}$	$\tau_{\mathrm{des}\,2}$	$\tau_{\mathrm{des}\,3}$	$\tau_{\mathrm{nuc}\,n}(s)$ ($n = 1, 2, 3$)	$\tau_{\mathrm{nuc}\,1}(f)$	$\tau_{\mathrm{nuc}\,2}(f)$	$\tau_{\mathrm{nuc}\,3}(f)$	Lines
MOVPE	1.0×10^{-3}	1.0×10^{-3}	1.0×10^{-3}	1.0×10^{-2}	1.0×10^{-2}	1.0×10^{-2}	1.0×10^{-6}	1.0×10^{-6}	1.0×10^{-6}	1.0×10^{-6}	(A)
ALE (1-ML)	1.0×10^{-3}	1.0×10^{-3}	1.0×10^{-2}	1.0×10^{-2}	5.5×10^{-3}	5.5×10^{-3}	1.0×10^{-4}	1.2×10^{-6}	1.0×10^{-4}	1.0×10^{-4}	(B)
ALE (1- and 2-ML)	1.0×10^{-3}	1.0×10^{-3}	1.0×10^{-2}	1.0×10^{-2}	5.5×10^{-3}	5.5×10^{-3}	1.0×10^{-4}	1.2×10^{-6}	1.5×10^{-6}	1.0×10^{-4}	(C)
ALE (3-ML)	1.0×10^{-3}	1.0×10^{-3}	1.0×10^{-2}	1.0×10^{-2}	5.5×10^{-3}	5.5×10^{-3}	1.0×10^{-5}	5.0×10^{-6}	1.5×10^{-6}	1.0×10^{-5}	(D)

$$\frac{1}{\tau_{\mathrm{nuc}\ 2}} = \frac{1 - a_2/a_1}{\tau_{\mathrm{nuc}\ 2}(s)} + \frac{a_2/a_1}{\tau_{\mathrm{nuc}\ 2}(f)}, \tag{7}$$

$$\frac{1}{\tau_{\mathrm{nuc}\ 3}} = \frac{1 - a_3/a_2}{\tau_{\mathrm{nuc}\ 3}(s)} + \frac{a_3/a_2}{\tau_{\mathrm{nuc}\ 3}(f)}. \tag{8}$$

Without this approximation, gradual increase in growth rate from zero to 1-ML SLG mode as well as 1- to 2-ML SLG modes cannot be reproduced. As to the adsorption, $\tau_{\mathrm{ads}\ n}$ ($n = 1$ and 2) are kept equal to 1.0×10^{-3} s, being the same value as that used to reproduce the growth rate for MOVPE. For $\tau_{\mathrm{ads}\ n}$ ($n = 3$), we end up with 1.0×10^{-2} s. This suggests the difference in the decomposed/adsorbed species between $n = 1$, 2 and $n = 3$. With these conditions, we have fit the data using $\tau_{\mathrm{des}\ n}$, $\tau_{\mathrm{nuc}\ n}(s)$ and $\tau_{\mathrm{nuc}\ n}(f)$ as fitting parameters. We first obtain $\tau_{\mathrm{des}\ n} = 1.0 \times 10^{-2}$ s for $n = 1$ and 5.5×10^{-3} s for $n = 2$, 3, respectively. $\tau_{\mathrm{des}\ 2}$ and $\tau_{\mathrm{des}\ 3}$ appear to be faster than $\tau_{\mathrm{des}\ 1}$, being consistent with the chemical trend that Al–Al bonding energy is weaker than that of the Al–As bonding. Next, we did a fine tuning with parameters $\tau_{\mathrm{nuc}\ n}(s)$ and $\tau_{\mathrm{nuc}\ n}(f)$. The best fit gives $\tau_{\mathrm{nuc}\ n}(s)$ to be 1.0×10^{-4} s for all n, and most importantly, $\tau_{\mathrm{nuc}\ n}(f)$ to be 1.2×10^{-6}, 1.0×10^{-4} and 1.0×10^{-4} s for $n = 1$, 2 and 3, respectively. In total, the differences in $\tau_{\mathrm{nuc}\ n}(f)$ and $\tau_{\mathrm{des}\ n}$ ($\tau_{\mathrm{nuc}\ 1}(f) \ll \tau_{\mathrm{nuc}\ 2,3}(f)$ and $\tau_{\mathrm{des}\ 1} > \tau_{\mathrm{des}\ 2,3}$) indicate that the first ML is formed preferentially compared with higher-order MLs, which is consistent with the adsorbate inhibition model for 1-ML SLG. The calculated fitting curve (B) shown in Fig. 8a together with experimental data visually shows this important point. When $\tau_{\mathrm{nuc}\ n}(f)$ for $n = 2$ is decreased from 1.0×10^{-4} to 1.5×10^{-6} s, the growth saturation for both 1- and 2-ML is clearly reproduced (Fig. 8b, line (C)). This suggests that the transition from 1- to 2-ML SLG mode at $T_s = 480°C$ is rather well explained by the model shown in Fig. 6. As to the 3-ML growth saturation, this calculation is not sufficient to reproduce the experimental data. Marginal fitting is obtained when $\tau_{\mathrm{nuc}\ n}(s)$ for all n are changed from 1.0×10^{-4} to 1.0×10^{-5} s, and $\tau_{\mathrm{nuc}\ n}(f)$ is selected to be one order of magnitude faster than 1- and 2-ML SLG mode. On the other hand, SLG for 1- and 2-ML cannot be reproduced in this case (Fig. 8c, line (D)). This result indicates that the contribution of $\tau_{\mathrm{nuc}\ 3}(f)$ becomes rather important, as discussed in the previous section. That the $\tau_{\mathrm{nuc}\ n}(s)$ becomes faster indicates the enhanced migration rate of adsorbed species, which is probably consistent with the metallic characteristics of the surface.

5. Conclusions

We have investigated ALE-AlAs using EDMAAl as an aluminum source. The existence of one, two and three monolayer self-limiting growth (SLG) saturation are established by systematically studying the growth behavior. For 1-ML SLG mode, carbon concentration in AlAs epilayers decreases with increasing growth temperature. This trend is completely reversed for 3-ML SLG mode. As to the 2-ML SLG mode, we have observed a mixed behavior of 1- and 3-ML SLG mode. The experimental results are explained in terms of the differences in surface condition and carbon incorporation associated with the surface. The 1-ML SLG mode is described by the conventional adsorbate inhibition model, whereas the 2- and 3-ML SLG modes are explained by the formation of metallic Al layers whose atomic configuration depends sensitively on substrate temperature.

Acknowledgements

The authors are deeply indebted to Professor Emeritus H. Kukimoto for continuous encouragement and valuable discussion. We also thank Dr. N. Kano for fruitful discussion especially about numerical calculation. We are also grateful to Taiyo-Toyo Sanso Co., Ltd. for supplying highly-pure AsH_3 gas. This work is supported in part by Research Fellowships of the Japan Society for the Promotion of Science for Young Scientists.

References

[1] T. Suntola, in: D.T.J. Hurle (Ed.), Handbook of Crystal Growth, vol. 3, chap. 14, Elsevier, Tokyo, 1994, p. 601.

[2] M. Pessa, P. Huttunen, M. Herman, J. Appl. Phys. 54 (1983) 6047.

[3] J. Nishizawa, T. Kurabayashi, J. Crystal Growth 93 (1988) 98.
[4] K. Kodama, M. Ozeki, K. Mochizuki, N. Ohtsuka, Appl. Phys. Lett. 49 (1986) 656.
[5] A. Doi, Y. Aoyagi, S. Namba, Appl. Phys. Lett. 49 (1986) 785.
[6] H. Ohno, S. Ohtsuka, A. Ohuchi, Y. Matsubara, H. Hasegawa, J. Crystal Growth 93 (1988) 342.
[7] M.L. Yu, U. Memmert, T.F. Kuech, Appl. Phys. Lett. 55 (1989) 1011.
[8] M. Ozeki, N. Ohtsuka, Appl. Surf. Sci. 82/83 (1994) 228.
[9] H. Yokoyama, M. Shinohara, N. Inoue, Appl. Phys. Lett. 60 (1992) 377.
[10] K. Fujii, I. Suemune, M. Yamanishi, Appl. Phys. Lett. 62 (1993) 1420.
[11] M. Ishizaki, N. Kano, J. Yoshino, H. Kukimoto, Thin Solid Films 225 (1993) 74.
[12] S. Hirose, N. Kano, M. Deura, K. Hara, H. Munekata, H. Kukimoto, Jpn. J. Appl. Phys. 34 (1995) L1436.
[13] N. Kano, S. Hirose, K. Hara, H. Munekata, H. Kukimoto, Appl. Phys. Lett. 65 (1994) 1115.
[14] N. Kano, S. Hirose, K. Hara, H. Munekata, H. Kukimoto, Appl. Surf. Sci. 82/83 (1994) 132.
[15] G. Landgren, R. Ludeke, C. Serrano, J. Crystal Growth 60 (1982) 393.
[16] T. Yao, H. Nakahara, H. Matuhata, Y. Okada, J. Crystal Growth 111 (1991) 221.
[17] H. Nakahara, H. Matsuhata, Y. Okada, T. Yao, Appl. Phys. Lett. 58 (1991) 1970.
[18] N. Maeda, M. Kawashima, Y. Horikoshi, J. Appl. Phys. 74 (1993) 4461.
[19] K. Ohta, T. Kojima, T. Nakagawa, J. Crystal Growth 110 (1991) 509.